Biomechanical Guidance System for Periacetabular Osteotomy

14

Mehran Armand, Robert Grupp, Ryan Murphy, Rachel Hegman, Robert Armiger, Russell Taylor, Benjamin McArthur, and Jyri Lepisto

Abstract

This chapter presents a biomechanical guidance navigation system for performing periacetabular osteotomy (PAO) to treat developmental dysplasia of the hip. The main motivation of the biomechanical guidance system (BGS) is to plan and track the osteotomized fragment in real time during PAO while simplifying this challenging procedure. The BGS computes the three-dimensional position of the osteotomized fragment in terms of conventional anatomical angles and simulates biomechanical states of the joint. This chapter describes the BGS structure and its application using two different navigation approaches including optical tracking of the fragment and x-ray-based navigation. Both cadaver studies and preliminary clinical studies showed that the biomechanical planning is consistent with traditional PAO planning techniques and that the additional information provided by accurate 3D positioning of the fragment does not adversely impact the surgery.

Keywords

Developmental dysplasia of the hip (DDH) · Periacetabular osteotomy (PAO) · Biomechanical guidance system · X-ray-based navigation

M. Armand (✉)
Johns Hopkins University Applied Physics laboratory, Laurel, MD, USA

Department of Mechanical Engineering, Johns Hopkins University, Baltimore, MD, USA

Department of Orthopaedic Surgery, Johns Hopkins University, Baltimore, MD, USA
e-mail: Mehran.Armand@jhuapl.edu

R. Grupp · R. Taylor
Department of Computer Science, Johns Hopkins University, Baltimore, MD, USA

R. Murphy · R. Armiger
Johns Hopkins University Applied Physics laboratory, Laurel, MD, USA

R. Hegman
Johns Hopkins University Applied Physics laboratory, Laurel, MD, USA

Department of Computer Science, Johns Hopkins University, Baltimore, MD, USA

B. McArthur
Dell Medical School at the University of Texas, Austin, TX, USA

J. Lepisto
Orton Orthopaedic Hospital, Helsinki, Finland

14.1 Introduction

Hip dysplasia is a condition in which the acetabulum is shallow and its roof is obliquely inclined laterally. As a result of this configuration,

G. Zheng et al. (eds.), *Intelligent Orthopaedics*, Advances in Experimental Medicine and Biology 1093, https://doi.org/10.1007/978-981-13-1396-7_14

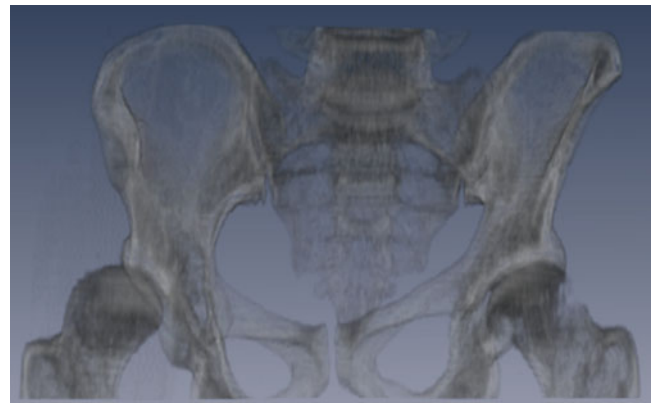

Fig. 14.1 Dysplastic right hip with inadequate coverage of the femoral head

the anterior and superior aspect of the articular cartilage of the femoral head is not adequately covered (Fig. 14.1). This leads to abnormally high stresses on the lateral edge of the acetabulum, a situation that may cause osteoarthritis [1, 2], fracture of the rim of the acetabulum due to excessive loading, and/or breakdown of the rim of the acetabular cartilage [3]. The symptoms of hip dysplasia usually occur in adolescents and young adults (<45 years) with seven times more incidence in females. If these patients were treated with total hip replacement (THR), they may require multiple revision surgeries during their lifetime. Each revision surgery will become substantially more invasive and challenging. Osteotomy of the hip, therefore, is commonly the surgery of choice for young adults suffering from dysplasia. Numerous outcome studies performed during the last 30 years have shown that performing periacetabular osteotomy (PAO) on young adults with dysplasia is a very effective surgery and prevents or delays osteoarthritis of the hip (e.g., [4, 5]).

The Bernese periacetabular osteotomy (PAO), one of the most popular techniques for periacetabular osteotomy, aims at achieving optimum coverage of the femoral head by recreating the relatively normal anatomy and mechanics for the dysplastic hip. This procedure can be performed without compromising pelvic ring stability (Fig. 14.2). It consists of a sequence of cuts through the ischium, pubis, and ilium. The procedure completely detaches the acetabulum from the rest of the pelvis (Fig. 14.2). The cup is then reoriented

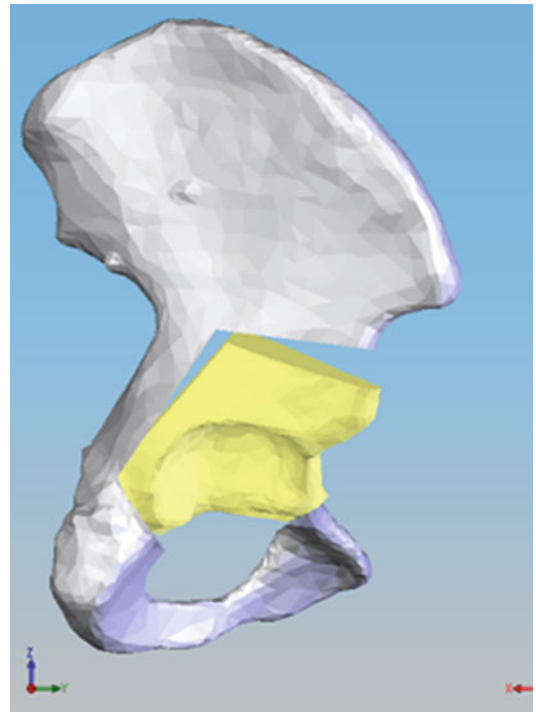

Fig. 14.2 Bernese PAO: the acetabular fragment (yellow) is osteotomized while maintaining pelvic stability

and fixed to the pelvis to improve the femoral head coverage and contact pressure distribution in the hip joint.

PAO is a technically challenging procedure with a steep learning curve [6–8]; the acetabular fragment must be detached with a limited line of sight and without fracture of the posterior column or damage to the hip joint (Fig. 14.2). There is always potential to damage the

neural and vascular structures close to the site of surgical activity [9]. Correct intraoperative 3D joint alignment is especially difficult [10] and should be checked intraoperatively to improve survivorship [11, 12]. Conventional procedures rely on limited feedback (typically, C-arm x-ray images and surgeon experience) for optimal joint alignment during the procedure. Previous systems have been developed to navigate tools during PAO [13, 14], which can help the surgeon in making the difficult cuts that do not allow a direct line of sight. However, those systems only address the technical challenge of surgically releasing the acetabulum and do not provide information regarding achieving the surgical goals for intraoperative joint alignment. Because of the limited advantage, additional equipment cost, additional time needed during the intervention, and space constraints in the operating room (occluding the field of view for optical trackers), at this time, few surgeons in the world perform image-guided computer-assisted PAO.

Several studies have proposed computer-assisted surgery for PAO (e.g., [13–16]) and described a number of potential benefits, including preoperative planning, and visual feedback combined with intraoperative navigation. However, the main limitation of each system is either the lack of fragment tracking or the inability to intraoperatively assess fragment location. Real-time feedback of the joint alignment and simulated joint contact pressures has the potential to provide the surgeon with necessary information to select and achieve optimal joint alignment [12, 17–20].

In this chapter, we describe our efforts in the development of a navigation system enabling tracking of the detached bone fragment and algorithms performing real-time biomechanical and geometrical analysis, providing the surgeon with anatomical measurements previously unavailable [21–25]. To this end, the system has successfully been used in 12 clinical investigations by Dr. Lepisto at Orton Orthopaedic Hospital, Helsinki, Finland, and 10 clinical investigations by Dr. Kjeld Soballe at Aarhus University Hospital, Denmark. We further discuss our more recent efforts to address the disadvantages due to the use of optical tracking by applying x-ray-based biomechanical navigation and 3D fragment tracking.

14.2 Overview of the System Architecture

The workflow of the biomechanical guidance system (BGS) workstation is shown in Fig. 14.3 and described below. Preoperatively, the partial CT around the hip joint and a standing radiograph of the full pelvis is acquired (Fig. 14.3a). Using the statistical atlas of dysplastic pelves, the 3D model of the (full) pelvis of the patient is reconstructed (Fig. 14.3b) [26, 27, 29]. The BGS workstation segments and reconstructs the acetabular cartilage from CT data and automatically calculates the radiographic angles [22] (Figs. 14.3c and 14.4). The workstation will also calculate the contact pressure distribution around the joint for simulated walking, standing, and sitting scenarios [18] (Fig. 14.3c). In the BGS simulation/visualization environment, the surgeon can manually or automatically find the optimized joint position for the PAO surgery and plan the osteotomy lines (Fig. 14.3h). Intraoperatively, The BGS can use two different methods for tracking the position of osteotomized bone fragment.

1. *Navigation using optical tracking:* The BGS can use an optical tracking system for tracking the fragment position and calculating the anatomical realignment angles. The surgeon creates at least three bone burs on the fragment and finds its position using a digitizer probe tracked by an optical tracker (Polaris, NDI Inc.) (Fig. 14.3e1) with respect to a reference rigid body attached to the pelvis. The details of the approach can be found in [30].
2. *X-ray-based navigation:* Before performing the osteotomy and after making skin incisions, the surgeon can inject 1 mm diameter tantalum radiopaque fiducials (shown as dots in Fig. 14.3e2) into the pelvis in the ilium (sta-

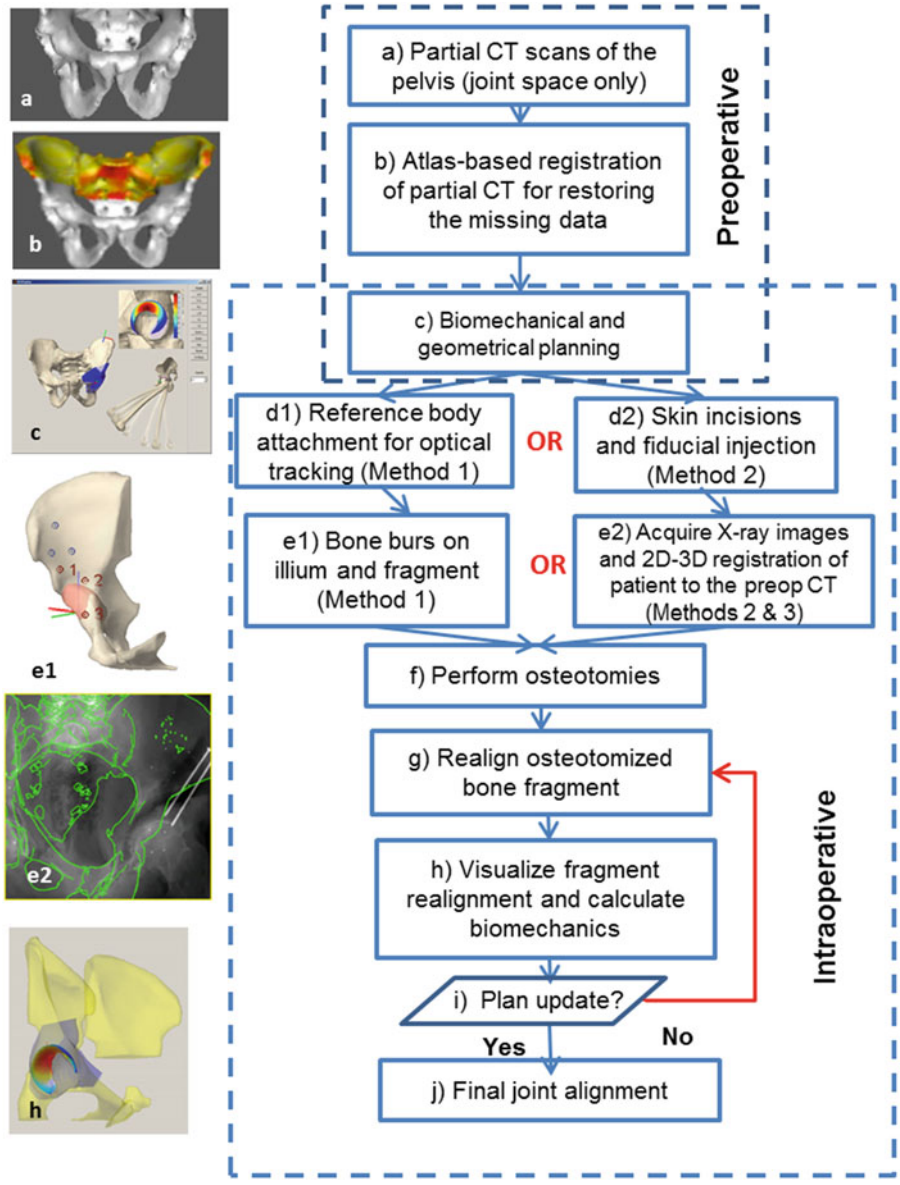

Fig. 14.3 BGS workflow with the use of two different methods for intraoperative navigation: (1) use of optical tracker, (2) x-ray-based navigation with fiducials

tionary fragment) and into the bone around the acetabular joint (the detached acetabular fragment) using a bead injector (Halifax Biomedical Inc.). The surgeon will then acquire two x-ray images, and the BGS workstation will perform 2D-3D registration to register the x-ray image to the preoperative 3D model of the pelvis and localize the fiducials on the model coordinates frames (Fig. 14.3e2). At any time after performing the osteotomies, the surgeon can acquire an x-ray image and the BGS workstation will then register the image to the 3D model using the fiducials on the stationary fragment. It will also determine the

change in relative coordinates of the fiducials on the detached fragment with respect to the fiducials in the stationary fragment and use the information to calculate the joint realignment angles and simulate the joint contact pressures (Fig. 14.3h) [31].

In general, the surgeon may need to consider trade-offs and revise the surgical plan (Fig. 14.3i) for a variety of reasons (e.g., patient bone quality, the strength of soft tissues around the joint, variability of the bone fracture line due to chiseling). The BGS will allow the surgeon to update the plan and recalculate the biomechanics and new joint angles when using any of the above approaches. In the following we describe the BGS modules and the evaluation experiments performed for each module and the overall system.

14.3 Planning Module

The planning module performs three tasks: (1) estimates the full pelvis shape from the partial CT scans of the pelvis around the hip joint with the help of a statistical atlas of dysplastic hips, (2) automatically calculates the conventional anatomical angles (Fig. 14.4) and simulated contact pressures (Fig. 14.3h) used for diagnosis of dysplasia, and (3) determines the desired joint realignment and osteotomy lines based on optimizing anatomical angles and joint contact pressure.

14.3.1 Pelvis Shape Estimation

The hip osteotomy patient demographic consists mainly of young (likely less than 45 years old) females without arthritis [9, 32]. Excess radiation is a cause for concern among all patients, especially those in this demographic group. Ideally, for the diagnosis of dysplasia and conventional planning of PAO, a partial CT around the hip joint is required. However, for biomechanical planning and intraoperative registration as used for computer-aided surgery procedures, a full pelvis CT will be more desirable.

We have developed two approaches for extrapolating the missing pelvis anatomy using statistical atlases. In the approach described in [26], we performed a study by constructing a statistical atlas of 104 normal male pelves using the process described in [33]. In this study the model representation for the atlas consisted of a tetrahedral mesh parameterizing the anatomical shape and Bernstein polynomials approximating CT intensities [34, 35]. We created partial CT data from the full CT by manually segmenting the partial volume and randomly sampling the segmented volume. The registration of partial CT to the statistical atlas consisted of rigid registration and principal component mode matching. We also used an image-based 2D-3D registration method with a standing AP radiograph with the 3D predicted model to see the effect of additional information on estimation accuracy. Using leave-out experiments, simulation results show that the accuracy of the atlas-extrapolated model improved and was comparable with the full CT model when x-ray images were used [26].

One of the issues with the above model is the discontinuity in transition from the actual CT data to the interpolated portion of the data. To address this issue, we developed a smooth extrapolation technique leveraging a partial pelvis CT and a statistical shape model of the full pelvis in order to estimate a patient's complete pelvis. Unknown anatomy was simulated by keeping the axial slices of the patient's acetabulum intact and varying the amount of the superior iliac crest retained, from 0 to 15% of the total pelvis extent. The smooth technique showed an average improvement over the cut-and-paste method of 1.31 mm and 3.61 mm, in RMS and maximum surface error, respectively [29, 36].

As another approach, we developed a robust, automated atlas-to-patient registration algorithm by using statistics of the voxel-wise *displacement* learned from computed deformation vectors on a training dataset. This allows direct translation of the template image to the patient image. Also, the voxel-wise displacement approach is a more natural fit for the goal of extrapolation of missing data from the atlas since it does not require the intermediate step of modifying/manipulating

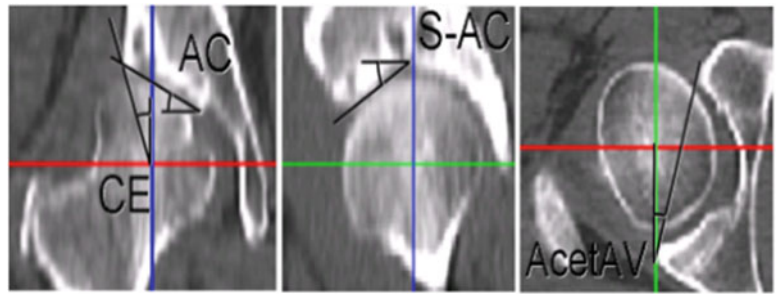

Fig. 14.4 Characteristic anatomical angles for diagnosis of dysplasia and conventional planning of PAO

the tetrahedral meshes. The details of the approach were reported in [27]. Briefly the leave-one-out experiments demonstrated 4.13 mm error with respect to the true displacement fields.

14.3.2 Geometrical and Biomechanical Planning

The BGS uses meshed surface models generated from the segmented CT scans of the pelvis to visualize patient anatomy and plan the location of the osteotomies. The articular surface of the cartilage model is developed on reformatted oblique CT slices extending radially from the center of femoral head as described in [22]. The biomechanical model uses linear [18] or nonlinear [37] discrete element analysis (DEA), with and without the measure of the cartilage thickness [25] to estimate contact pressures. Briefly, this approach models the cartilage region with a series of elastic compressive elements assuming no deformation of the acetabular bone in response to load. Loads are applied through the center of the femoral head to simulate standing [17] and the peak forces during walking and sitting down [38]. The parameters calculated in the mechanical analysis include metrics for both the location and magnitude of the peak contact pressure, as well as the hip range of motion (Fig. 14.3c). The biomechanical planning system was evaluated on 12 patients with developmental hip dysplasia. Consistent with 2-year outcome studies, the results showed that in all but one patient, the peak contact pressure significantly reduced postoperatively. The range of contact pressures reported preoperatively was 1.9 to 7.7 MPa, while postoperatively the range showed an improvement of 1.4 to 3.2 MPa. The details of this study were reported in [18].

The BGS also performs geometric characterization of the acetabulum using radiographic angles measured through CT reformats and x-ray projections (Fig. 14.4). The angles include the center edge (CE), acetabular inclination (AC) in the frontal plane, superior-anterior coverage (S-AC) in the sagittal plane, and the acetabular anteversion (AcetAV) in the transverse plane (Fig. 14.4). The detail of the calculations of these angles by the BGS is reported in [30].

14.4 Navigation Module

The BGS tracks the osteotomized fragment throughout the procedure. In addition to visualization, the BGS quantitatively reports the position of the fragment and updates and compares the mechanical analysis with that of the plans. The two approaches used for the BGS navigation is as follows:

14.4.1 Navigation with Optical Tracker

For this approach, the surgeon mounts a reference rigid body (NDI Inc. Waterloo, Canada) to either the contralateral or ipsilateral iliac crest using a 20 × 4 mm bone pin (Stryker, Kalamazoo, MI, USA). The BGS uses a two-stage process to register the subject-specific pelvis computer model developed from CT data to the patient. First, a coarse registration is performed by select-

ing anatomical landmarks in the CT model and by touching the corresponding landmarks on the patient's pelvis using a navigated digitizer probe.

Next, surface points are collected from patient's accessible bony regions using the navigated digitizer probe, and a fine point to surface registration is performed using iterative closest points (ICP) [39] or unscented Kalman filter (UKF) [40] technique. After registration, the surgeon creates and digitizes four burrs on the expected fragment (Fig. 14.3e1) to localize the fragment throughout the surgery. As the surgeon positions the fragment, at any time during the operation, he/she can touch the burs using the digitizing probe. The software will then recalculate and visualize the fragment position, simulate the magnitude and position of the peak contact pressure, and report both desired and actual anatomical characteristic angles. We performed a set of 19 cadaver studies to evaluate the system accuracy and refine the surgical protocol. Postoperative CT scans of the cadavers were obtained, and the accuracy of the intraoperative calculation of the angles was compared against the postoperative CT data. The results showed strong agreement (about 2 degrees) among intra- and postoperative angles in all three dimensions. The details of the work can be found in [30].

14.4.1.1 X-ray-Based Navigation

While the optical trackers have been shown to be reliable tools for the development of navigation systems for tracking the surgical tools in real time and tracking the detached bone fragment as discussed above, they suffer some disadvantages:

1. Surgeons are most accustomed to x-ray images and trust the images obtained by x-ray more than the visualization created from augmented reality using CT models and optical tracking.
2. Optical tracking requires additional reference bodies attached to the bone as well as specifically modified surgical tools.
3. Recent less invasive PAO surgeries with less than 10 cm skin incision (e.g., Dr. Soballe's approach [41]) will impose serious challenges to the use of optical trackers,especially for surface registration methods requiring exposure of considerable amount of pelvic bone surface.
4. The visualization based on optical tracking cannot substitute the need for x-ray images, as surgeons cannot reliably monitor some of the more challenging posterior osteotomy cuts via chiseling when using the virtual model.

The BGS can use an alternative approach for tracking the fragment and performing biomechanical guidance using x-ray images only. Tracking the acetabular fragment is essential to automated measurements of the anatomical angles and intraoperative biomechanical analysis without disrupting surgical workflow and eliminating the need for external tracking devices.

For x-ray-based navigation, after performing the skin incisions, the surgeon injects a series of radiopaque fiducials (1.0 mm diameter tantalum beads) to the stationary pelvis fragment (e.g., iliac wing) and the acetabular (moving) fragment similar to the approach approved for Roentgen stereometric analysis (RSA) using a bead injector (Halifax Biomedical Inc., Halifax, Canada) (Fig. 14.5). With the acetabulum intact and fiducials affixed, the surgeon acquires two to three x-ray images. A 2D-3D registration framework estimates the relative pose of the x-ray images and registering the patient anatomy of interest to the preoperative model obtained from CT scanner. Briefly, the registration framework is as follows:

1. Preoperatively acquired diagnostic CT data is converted into a volume image represented by line attenuation coefficients.
2. An initial estimate of the relative pose between each x-ray image and CT data will be used to start the registration process. This is achieved by determining some anatomical landmarks on the pelvis anatomy (e.g., ASIS, ISIS, etc.) and performing a point-based registration.
3. Digitally reconstructed radiographs (DRRs) will be generated from preoperative CT data using GPU-based implementation of the DRR using trilinear interpolation algorithm [42].

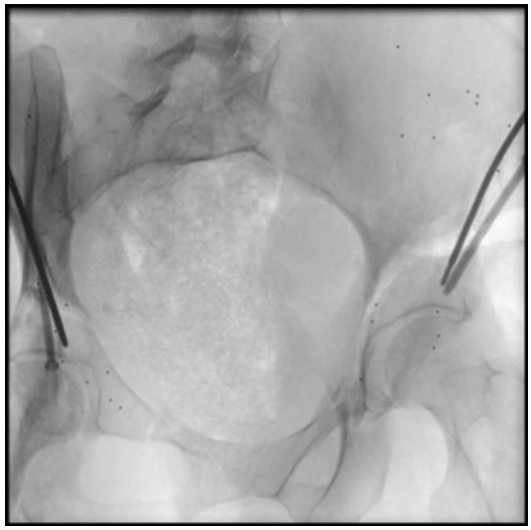

Fig. 14.5 The tantalum 1 mm beads (black dots) injected into the ilium and the detached acetabular fragment

4. A measure of similarity between x-ray images and DRR images (e.g., normalized cross-correlation of 2D Sobel gradients (Grad-NCC), gradient information (GI), or mutual information (MI)) is used as an objective function. A multi-resolution optimization approach maximizes the similarity between images.
5. After registration the corresponding location of each fiducial can be localized on the CT image, and the exact geometry of each of the two sets of fiducials (on stationary and moving fragments) can be determined.

For the first x-ray image set prior to osteotomy, the fiducials on the stationary fragment (ilium) define a common reference frame for future images, and the acetabular fragment fiducials define the initial fragment position. For intraoperative data, we can perform a feature-based registration [43] between the fiducials on the stationary fragment to align the current imaging frame with the preoperative imaging frame. The transformation of the fiducials on the acetabular fragment between pre- and intraoperative imaging frames quantifies the motion of the acetabular fragment. The system additionally provides the visualization of the current fragment location compared with the preoperative and planned location.

As mentioned above, the anatomical angles and biomechanics will be determined based on the new position of the acetabular fragment. If needed, the surgeon can update the surgical plan (due to the potential constraints), and the BGS workstation will intraoperatively update the target anatomical angles and biomechanics and allow the surgeon make the necessary trade-offs.

In a preliminary study, we attached eight stainless steel fiducials (four on the ilium and four around the hip joint) to a high-density plastic sawbone and performed PAO cuts around the hip joint. We obtained CBCT from the pelvis prior (preop) and after moving the acetabular fragment (postop). On four arbitrary x-ray images, we performed 2D-3D registration to find the transformation between the preop 3D model and the x-ray images. We then backprojected the fiducials in the x-ray images to obtain their 3D coordinates and compared it to the location of the fiducials on the acetabular (moving) fragment in postop CBCT (ground truth). We found a rotation error of 1.4 degrees which is within the acceptable error range (<3 degrees) for acetabular fragment placement [31].

14.5 Clinical Experience

In addition to multiple cadaver studies, the BGS with optical tracking has been used to perform a series of 12 consecutive PAO surgeries on 11 patients (including a bilateral PAO) at Orton Orthopaedic Hospital in Helsinki, Finland (approved by JHM IRB #NA_00001257), by Dr. Jyri Lepisto [44]. The patient cohort included 3 males and 8 females with the mean age of 34 (ranging from 22 to 28 years). For this study patients with concurrent femoral pathologies such as slipped capital femoral epiphysis or Legg-Calve-Perthes syndrome were excluded from the study.

For this study, the CT scans of pelves with 2 mm spacing between slices were obtained

prior to the surgeries. The CT images were then resampled and segmented with 1 mm slices. The points along acetabular rim were then digitized to develop the acetabular contact surface using lunate trace method as described in [22].

For these surgeries, following an incision on the iliac crest, the surgeon attached a removable rigid body (RB) to the contralateral iliac crest using an anchoring pin. Prior to any osteotomy, the surgeon digitized three landmarks on the pelvis (the ASIS and AIIS on the ipsilateral side and the ASIS on the contralateral side) that were previously defined in the CT model. After osteotomizing the anterior inferior iliac spine as part of the exposure, a bone burr was used to create a set of four 1.5 mm concavities on the iliac cortex (so-called confidence points similar to Fig. 14.3e). A coarse registration was then performed using the above three landmarks. Next, the surgeon collected a series of points on the exposed portions of pelvis. The data acquired was used to perform fine registration using iterative closest point [39] and/or unscented Kalman filters [40]. After registration the surgeon created two osteotomy cuts without repositioning the fragment. He then created four additional bone burrs on the osteotomized fragment. After performing osteotomies, the surgeon released and repositioned the fragment. He then assessed the position of the fragment by placing a digitizing probe on each of the four bone burr concavities in the fragment. The BGS used this data to calculate the 3D position of the fragment, the anatomical angles (Fig. 14.4), and the simulated contact pressure distribution on the articular joint (Fig. 14.3e1). The data was then compared with the preoperative plan.

To validate the BGS tracking, we compared intraoperative measurements to postoperative CT scans taken at least 4 months after each surgery. Overall, the BGS data acquisition did not introduce any major difficulties for the surgeon. The surgical time was comparable to the conventional approach (ranging from 95 to 210 min). The BGS measured fragment positioning was in good agreement with the postoperative CT measurements performed 4 months later (mean 3.7 degrees). The details of the clinical experience were reported in [44].

14.6 Limitations and Ongoing Work

The BGS addresses some of the existing challenges in performing PAO including steep learning curve, limited line of sight, limitation of current conventional methods for three dimensional tracking of the osteotomized fragment position, and lack of intraoperative biomechanical analysis tools. Notably, the system allows the surgeon to perform real-time analysis and update of the surgical plan as needed. Several aspects of the BGS can be improved with additional research. The biomechanical analysis is based on the simulation of the contact pressure. Our biomechanically based simulation for the correction of the joint position is commonly in agreement with the established ideal ranges for characteristic angles (current gold standards). The simulation methods used, however, can be considered the first order of approximation of the acetabular joint contact pressure. Addition of more details to the biomechanical model (e.g., modeling the effect of labrum, cartilage thickness, etc.) may further help to improve the accuracy of the outcome predictions. Moreover, the addition of details to the model must be validated against more sophisticated cadaveric experimentations and multiyear outcome studies on patients undergoing PAO.

The BGS supports navigation using both optical trackers and fluoroscopic C-arm. Our ongoing work has shown the promise of x-ray-based navigation with fiducials. However, image-based navigation system without the use of fiducials seems to be a more promising approach. Our very recent work demonstrates that if the PAO cuts closely follow that of the preoperative plan, the osteotomized fragment position can be successfully tracked at any time during the surgery by performing 2D-3D registration on 2–3 x-ray images. Furthermore, our current work focuses on showing that approaches for intraoperatively updating the preoperatively planned PAO cuts may also help in eliminating the use of fiducials

by improving the fragment model accuracy. The accuracy of the latter technique is currently under investigation.

Acknowledgments The human subject research and cadaver studies were approved by Johns Hopkins Medicine JHM IRB NA_00001257 and JHM IRB1 #05-09-02-01.The study was supported by grant number R01 EB60389 and R21 EB020113 from the National Institute for Biomedical Imaging and Bioengineering (NIH/NIBIB) and two JHU/APL graduate student scholarships.

References

1. Wiberg G (1939) Studies on dysplastic acetabula and congenital subluxation of the hip joint with special reference to the complication of osteoarthritis. Acta Chir Scand 83
2. Cooperman DR, Wallensten R, Stulberg SD (1983) Acetabular dysplasia in the adult. Clin Orthop Relat Res:79–85
3. Matta JM, Stover MD, Siebenrock K (1999) Periacetabular osteotomy through the smith-Petersen approach. Clin Orthop Relat Res:21–32
4. Siebenrock KA, Scholl E, Lottenbach M, Ganz R (1999) Bernese periacetabular osteotomy. Clin Orthop Relat Res:9–20
5. Trumble SJ, Mayo KA, Mast JW (1999) The periacetabular osteotomy. Minimum 2 year followup in more than 100 hips. Clin Orthop Relat Res:54–63
6. Davey JP, Santore RF (1999) Complications of periacetabular osteotomy. Clin Orthop Relat Res:33–37
7. Hussell JG, Rodriguez JA, Ganz R (1999) Technical complications of the Bernese periacetabular osteotomy. Clin Orthop Relat Res:81–92
8. Trousdale RT, Cabanela ME (2003) Lessons learned after more than 250 periacetabular osteotomies. Acta Orthop Scand 74:119–126
9. Ganz R, Klaue K, Vinh TS, Mast JW (1988) A new periacetabular osteotomy for the treatment of hip dysplasias. Technique and preliminary results. Clin Orthop Relat Res:26–36
10. Troelsen A (2009) Surgical advances in periacetabular osteotomy for treatment of hip dysplasia in adults. Acta Orthop Suppl 80:1–33
11. Albers CE, Steppacher SD, Ganz R, Tannast M, Siebenrock KA (2013) Impingement adversely affects 10-year survivorship after periacetabular osteotomy for DDH. Clin Orthop Relat Res 471: 1602–1614
12. Troelsen A, Elmengaard B, Soballe K (2009) Medium-term outcome of periacetabular osteotomy and predictors of conversion to total hip replacement. J Bone Joint Surg Am 91:2169–2179
13. Langlotz F, Stucki M, Bachler R, Scheer C, Ganz R, Berlemann U et al (1997) The first twelve cases of computer assisted periacetabular osteotomy. Comput Aided Surg 2:317–326
14. Mayman DJ, Rudan J, Yach J, Ellis R (2002) The Kingston periacetabular osteotomy utilizing computer enhancement: a new technique. Comput Aided Surg 7:179–186
15. Akiyama H, Goto K, So K, Nakamura T (2010) Computed tomography-based navigation for curved periacetabular osteotomy. J Orthop Sci 15:829–833
16. Hsieh PH, Chang YH, Shih CH (2006) Image-guided periacetabular osteotomy: computer-assisted navigation compared with the conventional technique: a randomized study of 36 patients followed for 2 years. Acta Orthop 77:591–597
17. Armand M, Lepisto J, Tallroth K, Elias J, Chao E (2005) Outcome of periacetabular osteotomy: joint contact pressure calculation using standing AP radiographs, 12 patients followed for average 2 years. Acta Orthop 76:303–313
18. Armiger RS, Armand M, Tallroth K, Lepisto J, Mears SC (2009) Three-dimensional mechanical evaluation of joint contact pressure in 12 periacetabular osteotomy patients with 10-year follow-up. Acta Orthop 80:155–161
19. Hipp JA, Sugano N, Millis MB, Murphy SB (1999) Planning acetabular redirection osteotomies based on joint contact pressures. Clin Orthop Relat Res 364:134–143
20. Tsumura H, Kaku N, Ikeda S, Torisu T (2005) A computer simulation of rotational acetabular osteotomy for dysplastic hip joint: does the optimal transposition of the acetabular fragment exist? J Orthop Sci 10:145–151
21. Armand M, Armiger R, Waites M, Mears S, Lepisto J, Minhas D, et al (2006) A guidance system for intraoperatively updating surgical-plans during Periacetabular osteotomy: development and cadaver tests. In: CAOS, Montreal, Canada, 2006
22. Armiger RS, Armand M, Lepisto J, Minhas D, Tallroth K, Mears SC et al (2007) Evaluation of a computerized measurement technique for joint alignment before and during periacetabular osteotomy. Comput Aided Surg 12:215–224
23. Armand M, Lepistö J, Merkle A, Tallroth K, Liu X, Taylor R et al (2004) Computer-aided Orthopaedic surgery with near real-time biomechanical feedback. APL Tech Dig 25:242–252
24. Lepisto J, Armand M, Armiger R (2008) Periacetabular osteotomy in adult hip dysplasia - developing a computer aided real-time biomechanical guiding system (BGS). Suomen Ortopedia ja Traumatologia 31:186–190
25. Niknafs N, Murphy RJ, Armiger RS, Lepisto J, Armand M (2013) Biomechanical factors in planning of periacetabular osteotomy. Frontiers in bioengineering and biotechnology, vol 1
26. Chintalapani G, Murphy R, Armiger R, Lepisto J, Otake Y, Sugano N, et al (2010) Statistical Atlas based extrapolation of Ct data. In: SPIE medcial

imaging: visualization, image-guided procedures, and modeling, vol 7625
27. Otake Y, Murphy R, Grupp R, Sato Y, Taylor R, Armand M (2015) Comparison of optimization strategy and similarity metric in atlas-to-subject registration using statistical deformation model. In: SPIE medical imaging, Orlando, pp 94150Q-94150Q-6
29. Grupp R, Otake Y, Murphy R, Parvizi J, Armand M, Taylor R (2016) Pelvis surface estimation from partial CT for computer-aided pelvic osteotomies. Bone Joint J 98:55–55
30. Murphy RJ, Armiger RS, Lepisto J, Mears SC, Taylor RH, Armand M (Apr 2015) Development of a biomechanical guidance system for periacetabular osteotomy. Int J Comput Assist Radiol Surg 10: 497–508
31. Murphy R, Otake Y, Lepisto J, Armand M (2013) Computer-assisted x-ray image-based navigation of periacetabular osteotomy with fiducial based 3D acetabular fragment tracking. In: Proceedings of 13th annual meeting of the international society for computer assited orthopaedic surgery, Orlando, pp 59–61
32. Sierra RJ, Trousdale RT, Ganz R, Leunig M (Dec 2008) Hip disease in the young, active patient: evaluation and nonarthroplasty surgical options. J Am Acad Orthop Surg 16:689–703
33. Chintalapani G, Ellingsen LM, Sadowsky O, Prince JL, Taylor RH (2007) Statistical atlases of bone anatomy: construction, iterative improvement and validation. Med Image Comput Comput Assist Interv 10:499–506
34. Yao J, Taylor RH (2003) Non-rigid registration and correspondence finding in medical image analysis using multiple-layer flexible mesh template matching. Int J Pattern Recognit Artif Intell 17(7):1145–1165
35. Sadowsky O, Cohen JD, Taylor RH (2006 July) Projected tetrahedra revisited: a barycentric formulation applied to digital radiograph reconstruction using higher-order attenuation functions. IEEE Trans Vis Comput Graph 12:461–473
36. Grupp R, Chiang H, Otake Y, Murphy R, Gordon C, Armand M, et al (2015) Smooth extrapolation of unknown anatomy via statistical shape models. In SPIE medical imaging, Orlando, pp 941524–941524-10
37. Volokh KY, Chao EY, Armand M (Jun 2007) On foundations of discrete element analysis of contact in diarthrodial joints. Mol Cell Biomech 4:67–73
38. Heller M, Bergmann G, Deuretzbacher G, Durselen L, Pohl M, Claes L et al (2001) Musculo-skeletal loading conditions at the hip during walking and stair climbing. J Biomech 34:883–893
39. Besl PJ, McKay ND (1992) A method for registration of 3-D shapes. In: IEEE Trans Pattern Anal Mach Intell 14:239–256
40. Moghari MH, Abolmaesumi P (2005) A novel incremental technique for ultrasound to CT bone surface registration using unscented Kalman filtering. Med Image Comput Comput Assist Interv 8:197–204
41. Troelsen A, Elmengaard B, Soballe K (Mar 2008) A new minimally invasive transsartorial approach for periacetabular osteotomy. J Bone Joint Surg Am 90:493–498
42. Otake Y, Armand M, Armiger R, Kutzer M, Basafa E, Kazanzides P et al (2012) Intraoperative image-based multi-view 2D/3D registration for image-guided Orthopaedic surgery: incorporation of fiducial-based C-arm tracking and GPU-acceleration. IEEE Trans Med Imaging 31:948–962
43. Kang X, Armand M, Yoshito O, YAU W, Cheung P, Hu Y et al (2014) Robustness and accuracy of feature-based single image 2D-3D registration without correspondences for image-guided intervention. IEEE Trans Biomed Eng 61:149–161
44. Murphy RJ, Armiger RS, Lepistö J, Armand M (2016) Clinical evaluation of a biomechanical guidance system for periacetabular osteotomy. J Orthop Surg Res 11:36